

Enhanced diffusion with abnormal temperature dependence in underdamped space-periodic systems subject to time-periodic driving

I. G. Marchenko


*NSC “Kharkov Institute of Physics and Technology”, 1 Akademicheskaya street, Kharkov 61108, Ukraine
and Kharkov National University, 4 Svobody Square, Kharkov 61077, Ukraine*

I. I. Marchenko

NTU “Kharkov Polytechnic Institute”, 21 Frunze street, Kharkov 61145, Ukraine

A. V. Zhiglo*

*NSC “Kharkov Institute of Physics and Technology”, 1 Akademicheskaya street, Kharkov 61108, Ukraine
and Kavli Institute for the Physics and Mathematics of the Universe (WPI), The University of Tokyo, Kashiwa, Chiba 277-8583, Japan*

 (Received 15 June 2016; revised manuscript received 26 November 2017; published 16 January 2018)

We present a study of the diffusion enhancement of underdamped Brownian particles in a one-dimensional symmetric space-periodic potential due to external symmetric time-periodic driving with zero mean. We show that the diffusivity can be enhanced by many orders of magnitude at an appropriate choice of the driving amplitude and frequency. The diffusivity demonstrates abnormal (decreasing) temperature dependence at the driving amplitudes exceeding a certain value. At any fixed driving frequency Ω normal temperature dependence of the diffusivity is restored at low enough temperatures, $T < T_{\text{TAD}}(\Omega)$ —in contrast with the problem with constant external driving. At fixed temperature at small driving frequency the diffusivity either slowly decreases with Ω , or (at stronger driving) goes through a maximum near Ω_2 , the reciprocal superdiffusion regime termination time. At high frequencies, between Ω_2 and a fraction of the oscillation frequency at the potential minimum, the diffusivity is shown to decrease with Ω according to a power law, with the exponent related to the transient superdiffusion exponent. This behavior is found similar for the cases of sinusoidal in time and piecewise constant periodic (“square”) driving.

DOI: [10.1103/PhysRevE.97.012121](https://doi.org/10.1103/PhysRevE.97.012121)

I. INTRODUCTION

The phenomena of diffusion and transport over a potential energy landscape play a key role in a number of processes in physics, chemistry, and biology [1–5]. Josephson tunneling junctions, superionic conductors, phase-locked-loop frequency control systems, and charge density waves are a few examples of systems in which these processes in periodic potential are important [6].

In recent years the interest has been growing to experimental studies of manipulating the particle diffusion by external fields. One can effectively control the diffusion processes by varying the field parameters. For instance, a huge enhancement in diffusivity (exceeding its value in the same system without extra driving by a factor of order hundreds) was observed in studying particle diffusion in colloids with optical traps (optical vortices) [7]. A large increase in diffusivity was also observed in studies of paramagnetic particle diffusion on surfaces of garnet ferrites influenced by external time-periodic magnetic field [8]. In the same manner diffusivity growth with shaking strength was noticed in experiments with granular gas [9]. It became possible to increase the diffusivity of ions in membrane channels by varying the external electromagnetic field

[10]. One can increase the rates of diffusion-limited physical processes, and effectively separate micro- and nanoparticles of different nature by varying diffusion coefficients in different directions [11].

Despite these remarkable achievements, a quantitative description of such enhanced diffusion under the influence of external forces remains fragmentary to date. The present study contributes to this subject, with a focus on systems under time-periodic driving.

A. Diffusion of Brownian particles in spatially periodic potentials under constant external driving

A typical model considered is an ensemble of Brownian particles in a periodic potential subject to external driving F_t . Dynamics of the particles can be described by the Langevin equation

$$m\ddot{x} = -dU(x)/dx - \gamma\dot{x} + F_t(t) + \xi(t) \quad (1)$$

(in one dimension), where t is the time, x is the particle coordinate, m is its mass, and γ is the friction coefficient. The overdot stands for the time differentiation. $\xi(t)$ represents thermal fluctuations, in most studies considered Gaussian white noise with a certain temperature T . The potential energy $U(x)$ is periodic in x . In our study

$$U(x) = -(U_0/2) \cos(2\pi x/a), \quad (2)$$

*azhiglo@uchicago.edu

where a is the lattice constant and U_0 is the potential barrier height.

The lattice force F_{lat} acting upon the particle is

$$F_{\text{lat}}(x) = -dU/dx = -F_0 \sin(2\pi x/a). \quad (3)$$

The quantity $F_0 = \pi U_0/a$ coincides with the minimal external force needed to drag the particle over the potential barrier separating potential minima on the one-dimensional (1D) lattice at large friction.

Special cases of underdamped and overdamped physical systems are often considered. In overdamped systems inertial effects may be neglected, significantly simplifying the mathematical treatment of the problem. In underdamped systems on the other hand the viscous decay of oscillations occurs on times long compared with the oscillation period in the potential; such systems are harder to investigate, and the progress in studying these is more limited compared with overdamped ones.

The first detailed studies of a Brownian particle motion in a washboard potential (i.e., a periodic potential tilted with an additional constant force field, $dF_t/dt = 0$) for all values of the friction were carried out by Risken and co-workers [12,13]. It was shown that at low friction the appearance of “locked” (in which the particle oscillates around one minimum of the potential) and “running” (where the particle travels through many potential periods, not getting trapped at separate minima) solutions was important for the particle ensemble behavior. At small temperatures running solutions appear abruptly at the external force value exceeding certain critical F_{cr} ; at smaller forces a single class of solutions (locked) is realized. Systematization of the results of these studies may be found in Ref. [6].

The problem was studied by solving the Fokker-Planck equation (FPE) for the velocity and coordinate distribution function $\tilde{N}(V, x; t)$. One approach [12] involved an approximate solution by the matrix continued fraction method for the expansion coefficients of stationary $\tilde{N}(V, x)$ over an appropriate (infinite) complete set of functions. Two leading expansion coefficients could be obtained efficiently by that method, those sufficed for computing the particle flux (but not diffusion). Another approach [13] was used at low friction, in which case energy E was a slow variable [changing on the viscous dissipation time scales, whereas x oscillated with short period (9)]. The distribution function was rewritten in (E, x) variables, FPE was solved in these by perturbation expansion near the ansatz that depended on E only, valid at $\gamma = 0$. Diffusion properties remained not studied by either method at $F \neq 0$. This matter was partly addressed in other works, based on simulations of the stochastic Langevin equation.

Early systematic study of diffusion by means of numerical simulation of the Langevin equation in periodic potential with extra constant driving was undertaken in [14]. Costantini and Marchesoni analyzed both overdamped and underdamped settings. At low dissipation they observed significant enhancement of the spatial diffusion near the critical force F_{cr} ([14]; Fig. 1: diffusivity ten times larger than its postmaximum value at $F = 2F_{\text{cr}}$, at the temperature equal to 0.6 of the potential well depth U_0), and related that to features of the particle jump statistics and locked-to-running transition. Similar simulations were reported in [15] for driving with a time-periodic component.

Further progress in studies of the diffusion under the action of constant force was made in [16–18]. Time dependence of the particle ensemble dispersion was studied in [16]. It was shown that in underdamped systems a special regime of dispersionless transport was realized, in which dispersion virtually did not change with time, on a certain limited interval of time. The authors explained this phenomenon; they showed that strongly nonequilibrium distribution of particles in space (with steep front and exponential tail, formed as the particles first exit their original potential well) persisted for long times, before eventually broadening and assuming a normal Gaussian shape.

The temperature dependence of the diffusivity was studied as well [18]. The authors observed that the maximal diffusivity D_{max} was achieved near the F_{cr} . At low friction D_{max} was shown to depend abnormally on the temperature—increase with decreasing temperature T . Fitting, for the three temperatures studied, yielded $D_{\text{max}} \propto T^{-3.5}$ relation.

The presence of such abnormal temperature dependence is one important aspect in which underdamped systems differ from overdamped ones. In fact, certain peculiarities in diffusivity at low temperatures are observed (for driven Brownian particles in space-periodic potentials) in the overdamped situation as well. Reimann and co-workers [19] showed analytically that for a sinusoidal in space potential at external constant force value near F_0 , the force required for direct particle pull over the potential barrier, the ratio of D_{max} to the diffusivity value D_0 in the viscous medium without the lattice and bias forces grows at temperature decreasing $\propto T^{-2/3}$. Yet the diffusivity itself still vanishes at $T \rightarrow 0$, as $D_{\text{max}} \propto T^{1/3}$ [19], and grows monotonically with T for all T .

Regions in the parameter space in which $\partial D/\partial T < 0$ were found in the overdamped problem in [20] (cf. Fig. 6) for specially crafted exotic potentials, flat apart from narrow peaks. The authors linked the abnormal $D(T)$ dependence to the large ratio of relaxation to escape time in such a system. Similarly, abnormal $D(T)$ behavior was found in [21] (cf. Figs. 2–4) for piecewise linear potential at extreme asymmetry, essentially sawtooth. So, while possible at large friction, special atypical conditions must be met for the existence of parameters $\{F, T\}$ at which $\partial D/\partial T < 0$. On the contrary, such parameters exist universally in the problem with small friction ([22]; more below).

Another distinction of the diffusion behavior in the overdamped problem is that the maximum in $D(F)$ is achieved close to the F_0 , whereas at low friction $D_{\text{max}}(F)$ is achieved at (typically much smaller) F_{cr} .

The theoretical results for the overdamped setup were verified in a number of experimental studies. Diffusion of colloidal particles in a tilted periodic potential created with laser traps [23], Fig. 1, agreed reasonably well with the analytic [19] $D(F)$ dependence. The potential barrier height and the free diffusion coefficient were treated as fit parameters. Diffusivity in [24] varied nonmonotonically with F with a maximum near F_0 (Fig. 7), and agreed fairly well with the analytic predictions from [19]. The potential was inferred from an independent study of the colloidal particle spatial distribution function. In that work colloidal particles diffused over the potential created by the bottom grid of colloidal spheres; extra constant driving was due to gravity (controlled by the sample inclination angle). Different limiting cases of analytic predictions [19] for the mean particle velocity and diffusivity were compared with the

experimental results at different settings, and showed good agreement.

In underdamped systems the physical reason behind the abnormal temperature dependence of the diffusivity is traced to the jump length of running particles (before getting retrapped at another potential minimum) increasing with the temperature decrease [22], this phenomenon being absent in overdamped systems (as these have no proper running states, at $F < F_0$). The maximal diffusivity is achieved at driving near F_{cr} , as at this value populations of locked and running particles are about equal, and it is the mutual motion between these two populations (with temperature-independent running particle speed) that leads to fast spreading of the particle packet, manifested as a giant diffusion [18].

Thorough analysis of (the temperature and force dependence of) the diffusion in underdamped systems was carried out in [25]. Numerical simulations of the Langevin equation were performed for a wide range of the temperatures and driving F . The phenomenon of the diffusivity growth with the temperature decrease, in the current work called TAD, “temperature-abnormal diffusivity,” was shown to be manifested in a narrow interval of applied external driving values near F_{cr} . That interval is called region II in the present paper. Outside that interval, at weaker driving (region I) and stronger one (region III), the dependence of the diffusivity on the temperature was normal, increasing. It was demonstrated that in region II the diffusivity grew with the temperature decrease as $D_{max} \propto T^{2/3} \exp[\mathcal{E}/(k_B T)]$ for certain $\mathcal{E} > 0$ (k_B being the Boltzmann constant). Such a scaling was checked valid for a set of temperatures in $k_B T/U_0 \in [0.05; 0.85]$; whereas the power-law fit $D_{max} \propto T^{-3.5}$ proposed for TAD in [18] could approximate the results only in the narrow temperature interval investigated in [18]. We showed that the main exponential growth factor resulted from such an exponential growth of the correlation time τ_{corl} at the temperature decreasing, found by simulations.

Properties of the mobility and diffusion were further elucidated and systematized for a broad range of (constant in time) forces F , friction coefficients γ , and temperatures T in [22], in sinusoidal 1D potential in the underdamped setting. We observed that the distribution function of the particles in velocity space $N(V)$ [full distribution function in (x, V) averaged over oscillations in x] had a clear bimodal structure for F in region II, and could be approximated as a sum of two Gaussians,

$$N(V) = A \exp\left(-\frac{mV^2}{2k_B T}\right) + B \exp\left(-\frac{m(V - F/\gamma)^2}{2k_B T}\right). \quad (4)$$

Both Gaussians hence had the same width $(2k_B T/m)^{1/2}$ and were centered around $V_r = F/\gamma$ (running particles) and zero velocity (locked ones). One could expect Gaussian distributions near the maxima of the $N(V)$ on simple physical grounds, yet in fact the approximation above was quite accurate everywhere except the vicinity of the minimum between the two Gaussians, the region influenced by the particles transitioning between the locked and running populations. We also observed that in the corresponding deterministic problem the evolution of a certain slow velocity variable (maximal velocity of the particle in one oscillation period in the potential; slow in

the limit $\gamma \rightarrow 0$; related to the slow energy variable used by Risken and co-workers) could be represented as overdamped dynamics in a certain velocity potential $W_F(V)$. Extension of the dynamics equation for $V(t)$ to a setup with added white noise $\zeta(t)$,

$$\begin{aligned} \dot{V} &= -dW_F(V)/dV + \zeta(t), \\ \langle \zeta(t)\zeta(t') \rangle &= 2\gamma k_B T m^{-2} \delta(t - t'), \quad \langle \zeta(t) \rangle = 0, \end{aligned}$$

produced a distribution $N_W(V)$ with the same behavior near its two maxima as the bimodal $N(V)$ above, found by simulations of the full problem in the (x, V) phase space. The agreement with $N(V)$ was in fact good at most V , except the dubious area near the minimum of $N(V)$ separating the two maxima at $V = 0$ and F/γ .

The deficiency of our velocity potential model near the minimum in $N(V)$ was expectable from the approximate way we constructed the $W_F(V)$. The construction was based on the requirement for the deterministic $\dot{V} = -dW_F(V)/dV$ dynamics to reproduce correct relaxation of an arbitrary trajectory to the proper late-time asymptotic (locked or running, depending on the trajectory initial conditions). The relaxation dynamics was not well understood in the region close to $V \approx V_{cr}$ —the boundary value such that trajectories passing through the minimum of $U(x) - Fx$ at $t = 0$ with $V > V_{cr}$ evolved towards the running states, whereas those with $V < V_{cr}$ evolved towards the locked states. Consequently the potential proposed was by construction only reliable not too close to V_{cr} . That deficiency was manifested in several aspects; in particular we could not fix mutual normalization of the two Gaussians corresponding to locked and running populations from self-sufficient considerations. That normalization was fixed by requiring the agreement of the average $\langle V \rangle$ found from the theory based on the velocity potential with $\langle V \rangle$ found from direct Monte Carlo simulation of the full problem (1). The normalization factor turned elegant, independent of F and γ in the broad ranges studied. A simple fit, linear, was obtained for the (found numerically) V_{cr} dependence on F and γ .

With the fits proposed, $W_F(V)$ could be found in an explicit form for any $\{F, \gamma, T\}$ in the ranges studied. $N_W(V) = \exp[-m^2 W_F(V)/(\gamma k_B T)]$ reproduced well the distribution of solutions of (1), except at the $N_W(V)$ minimum. The diffusivity obtained from $N_W(V)$ through the Kubo relation agreed well with D found numerically by simulations of (1). Divergence of the correlation time τ_{corl} as an exponential of inverse temperature at $T \rightarrow 0$ found in [25] was explained, related to the Kramers rate of transitions in the velocity space between the locked and running populations through the potential barrier in $W_F(V)$. The fits are instrumental to comprehend the features of the transport and diffusivity in all the parameter space, and are useful for experimentalists.

B. Periodic in time external driving

In most practical applications periodic in time external forces (electromagnetic, acoustic, etc.) are more straightforward to implement than constant driving. It is natural to study how the findings for the constant driving problem are modified for the time-periodic driving setup, both from a theoretical and practical point of view. By changing the diffusivity with the aid of periodic external fields it is possible to create surface

structures with prescribed properties; influence the dynamics of point defects in crystals, under irradiation in part; alter the dislocation motion dynamics; increase chemical reaction rates in selected directions; manipulate the efficiency of processes in biological systems, to mention just a few applications [26,27].

A large fraction of the works on periodic driving deal with ratchet-type systems [4] or stochastic resonance. Studies focusing on diffusion properties in symmetric periodic systems are scarce. We are not aware of any works that systematically study the combined dependence of the diffusivity on the temperature, the driving amplitude, and the frequency in a representatively broad range of these parameters.

Dependence of the diffusivity on the interplay between the external periodic [piecewise constant, Eq. (7), below] driving and the lattice force was studied in [28] in a 2D overdamped setup. The driving frequency was fixed at one value. It was shown that in a system with a sum of Yukawa potentials at square grid nodes the particle diffusivity was significantly enhanced for certain intricate set of bands (“A-windows”) of the driving amplitudes and orientations with respect to the grid. At special driving arrangement TAD was observed for some diffusivity tensor components, and one of its principal values increased exponentially with inverse temperature. The other diffusivity tensor principal value decreased exponentially at the same time. It is likely that multidimensionality effects were crucial for TAD. Instead of having two, locked and running, populations in one dimension accounting for (already sophisticated in this case) diffusion features, flows in higher dimensional problems are more complex, known to result in further peculiarities in transport and diffusion [5,29].

An underdamped 1D system was studied in [30], with a sinusoidal in x potential (2) and sinusoidal in time driving. Diffusivity enhancement by orders of magnitude was seen. TAD was observed for some (low) driving frequencies, at the driving amplitude $0.15F_0$ studied. Dependence of the diffusivity on the driving frequency was studied in more detail in [31], and was shown to be nonmonotonic at large enough driving amplitudes ($0.15F_0$ and $0.25F_0$, at $k_B T/U_0 = 0.258$.) At $0.15F_0$ the maximum in the frequency dependence of the diffusivity $D(\Omega)|_{\{T,F\}=\text{const}}$ persisted for all the temperatures studied, corresponding frequency Ω_{max} increasing from $\sim 2 \times 10^{-4}$ to $\sim 6 \times 10^{-3}$ (in units of the frequency of small oscillations at the potential minimum in the absence of friction) at temperatures $k_B T/U_0 \in [0.129; 0.388]$. TAD was also spotted in [32] at the driving frequency modelled.

The goal of the present work is to investigate in detail the dependence of the diffusivity on the amplitude and the frequency of uniform time-periodic external driving in a 1D underdamped space-periodic system, and conditions under which TAD is realized. We mainly study piecewise constant periodic [PCP; Eq. (7)] driving as this case is more straightforward to relate to the results for constant driving. For such a PCP driving one might expect that in the limit $\Omega \rightarrow 0$ the $D(F, T)$ behavior must coincide with such in the constant driving problem, $D|_{\Omega=0}$. We show that in fact the convergence is not uniform in T , and at arbitrarily small Ω at temperatures below a certain Ω -dependent value the diffusivity behavior is qualitatively different from that in the constant driving problem.

$D(F, T)$ still behaves in three different ways in regions I–III of the driving amplitude. As in the constant driving

problem, in region I TAD is not observed, and D grows with F . Contrary to the situation in the constant driving setup TAD is observed in region III for a certain interval of frequencies. Both in regions II and III TAD is only realized in a finite interval of the temperatures, *bounded from below* by certain positive temperature $T_{\text{TAD}}(\Omega)$; at lower temperatures normal (increasing) temperature dependence of D is restored. The reason for this phenomenon, that at low temperatures the behavior differs from that in the constant driving problem, is related to the fact that the relaxation time of the particle distribution function diverges at $T \rightarrow 0$. At small enough T time π/Ω between the $F_t(t)$ sign switching is not long enough for the equilibrium distribution to be established. Particles are in the anomalous diffusion regime (e.g., superdiffusion) through the whole period of F_t oscillations, hence the resulting late time diffusion coefficient differs from $D|_{\Omega=0}$.

This interplay between the period of the driving and the intrinsic anomalous diffusion regime time span leads to relations between this time span, superdiffusion exponent α , and $D(\Omega)$. $D(\Omega)$ is shown to scale as a power of Ω in certain intervals of the frequency, limited on one side by the reciprocal anomalous diffusion regime time span; cf. Eqs. (16) and (18) below. The physics of the maximum [31] in $D(\Omega)|_{\{T,F\}=\text{const}}$ discussed above is explained in the same framework for F in region III (cf. Fig. 9). Presented results thus provide means for experimental studies of anomalous diffusion properties by probing long-time diffusivity as a function of the driving frequency.

We describe the methods used in Sec. II. In Sec. III we show how the diffusivity changes with the PCP driving frequency Ω , starting from the understood results at constant driving. We observe that TAD is realized for some (intermediate) driving amplitudes, in regions II and III. Section IV is devoted to studying the $D(T)$ behavior at fixed Ω . The results for the diffusivity in the case of sinusoidal in time driving are shown in Sec. V. We conclude in Sec. VI.

II. PROBLEM SETUP AND NUMERICAL METHOD

A. Problem setup

In this paper the Brownian motion is described by the Langevin equation (1), with thermal fluctuations $\xi(t)$ represented by Gaussian white noise with correlation

$$\langle \xi(t)\xi(t') \rangle = 2\gamma k_B T \delta(t - t'); \quad \langle \xi(t) \rangle = 0. \quad (5)$$

Here k_B is the Boltzmann constant, and T is the temperature. Angle brackets $\langle \dots \rangle$ with no subscripts mean averaging over the particle ensemble.

For physical values we use the same parameters as in [22], typical for adatom diffusion on close-packed metal surfaces. Namely,

$$U_0 = 80 \text{ meV}, \quad a = 2\text{\AA} \quad (6)$$

for the activation barrier and the lattice constant are adopted.

Two possibilities for the external periodic driving are studied: piecewise constant periodic (PCP) driving,

$$F_t(t) = F_e \text{sgn}[\sin(\Omega t)], \quad (7)$$

and the sinusoidal one,

$$F_t(t) = F_e \sin(\Omega t). \quad (8)$$

Ω is the angular frequency of the external force and F_e is its amplitude.

It is convenient to use dimensionless time t' and space coordinate x' , normalizing the physical values to the period of small oscillations,

$$\mathcal{T}_0 = 2\pi/\Omega_0 = a(2m/U_0)^{1/2}, \quad (9)$$

at the potential minimum in the absence of friction, and to the lattice spatial period a respectively:

$$t' = \frac{t}{\mathcal{T}_0} = \frac{t}{a} \sqrt{\frac{U_0}{2m}}, \quad x' = \frac{x}{a}. \quad (10)$$

Dimensionless temperature T' and friction coefficient γ' are further introduced:

$$T' = 2k_B T/U_0, \quad \gamma' = \gamma a(mU_0/2)^{-1/2}. \quad (11)$$

Equations (1) and (5) in these dimensionless units read

$$\begin{aligned} d^2 x'/dt'^2 &= -dV(x')/dx' - \gamma' dx'/dt' + F_t'(t') + \xi'(t'), \\ \langle \xi'(t'_1) \xi'(t'_2) \rangle &= 2\gamma' T' \delta(t'_1 - t'_2), \quad \langle \xi'(t') \rangle = 0, \end{aligned}$$

with dimensionless $F_t' = 2aF_t/U_0$, $\xi' = 2a\xi/U_0$, $V(x') = \cos(2\pi x')$.

Definitions (10) and (11) differ from such in [16,22,25,30,31,33] by extra factors of 2 appearing in the definition of t' , and consequently in T' and γ' as well. The current definition makes interpreting the results easier ($t' = 1$ corresponds to one oscillation period at small γ'). For more straightforward comparison with our previous works we also use another dimensionless temperature in the figures,

$$T^\dagger = k_B T/U_0 = T'/2.$$

The parameters of the dimensionless problem are F_e/F_0 , $\omega = \Omega\mathcal{T}_0$, γ' , T' .

Below lowercase ω 's (frequencies), and corresponding periods $\tau = 2\pi/\omega$ denote dimensionless quantities. Physical frequencies and periods are obtained by respectively dividing and multiplying these by the period \mathcal{T}_0 of small oscillations in the lattice potential at $\gamma = 0$.

The overdamped problem is characterized by $\gamma/m \gg \Omega_0$, whereas $\gamma/m \ll \Omega_0$ (equivalently, $\gamma' \ll 1$) corresponds to underdamped dynamics. We study the underdamped case here. The friction coefficient $\gamma' = 0.2$ we use corresponds to the same physical value as in earlier studies [22,25].

B. Numerical method

We solve the stochastic equation (1) and (5) numerically using a Verlet-type algorithm [34] with a time step Δt somewhat shorter than 1/100th of the period of oscillation \mathcal{T}_0 . The statistical averaging is performed over the ensemble consisting of at least $N = 5 \times 10^4$ particles. To verify the modeling consistency some computations were performed with $N = 5 \times 10^6$.

The initial conditions are set as follows. Each particle is placed at $x = 0$, its velocity chosen at random, with Maxwellian distribution for a given T . Thermalization over

100 oscillation periods, in the potential $U(x)$ but without the $F_t(t)$, is then used to get equilibrium particle distribution over both coordinate and velocity. Tests show that the distribution function does not change after that time. In the process of such thermalization the particles can jump to nearby elementary cells of the lattice. Such relocated particles are returned back to the initial cell by translation over an integer multiple of the lattice constant, to get diffusion of all particles starting from the initial cell of the lattice.

The diffusivity is computed based on the dispersion σ^2 of the particle distribution in the limit of large times:

$$D' = \lim_{t \rightarrow \infty} D'_{\text{eff}}(t) = \lim_{t' \rightarrow \infty} \frac{\langle (x' - \langle x' \rangle)^2 \rangle(t')}{2t'} \equiv \lim_{t' \rightarrow \infty} \frac{\sigma^2}{2t'}. \quad (12)$$

D' and σ are dimensionless in our notation. The physical diffusivity is $D = D'a^2/\mathcal{T}_0$.

For each diffusivity calculation we find time t'_{lin} , after which the dispersion grows linearly with time (if averaged over the driving period). The D' is calculated as $\sigma^2/(2t')$ at $t' = 100t'_{\text{lin}}$.

It is known that in systems with low dissipation transient regimes of anomalous diffusion can be realized [33], characterized by

$$\sigma^2 = \langle (x' - \langle x' \rangle)^2 \rangle \propto t'^{\alpha}. \quad (13)$$

The process with $\alpha > 1$ is referred to as superdiffusion, whereas subdiffusion is characterized by $\alpha < 1$. Distinct regimes of anomalous diffusion were observed in our simulations. The choice of initial conditions above aided in having these regimes in clear form.

We determine the exponents α by the least-square linear fitting between $\ln(\sigma^2)$ and $\ln t$ on the time interval of interest.

III. PIECEWISE CONSTANT PERIODIC DRIVING: DEPENDENCE OF THE DIFFUSIVITY ON THE DRIVING FREQUENCY

Qualitatively different functional dependencies $D(F, T)$ were shown in [25] to be realized at (constant in that study) $F_t(t) = F_e$ in regions I–III. Plots of the diffusivity as a function of the external force F_e at several temperatures [based on numerical simulations of $\sigma^2(t)$ in [25], recomputed for the current units] are shown in Fig. 1, top plot. For F_e in region I diffusion is enhanced as external force F_e value increases, whereas in region III diffusion is inhibited as F_e increases. In regions I and III D grows with T increasing. Contrary to this (normal temperature behavior) in region II D grows as T decreases. This is the region of “temperature-abnormal diffusivity” (TAD). The *diffusion process* at sufficiently late times is normal, $\sigma^2 \propto t^1$, however the *diffusion coefficient* $D' = \sigma^2/(2t')$ (abnormally) increases as the temperature decreases.

TAD is also possible at time-periodic external driving as it was seen in [30]. At such driving TAD was only observed in a finite interval of the driving frequencies. Studies were carried out at $F_e = 0.15F_0$, that would correspond to region III for the constant driving of the same amplitude (see Fig. 1), so TAD *would not* be observed at such F_e value were the driving $F_t(t)$ constant.

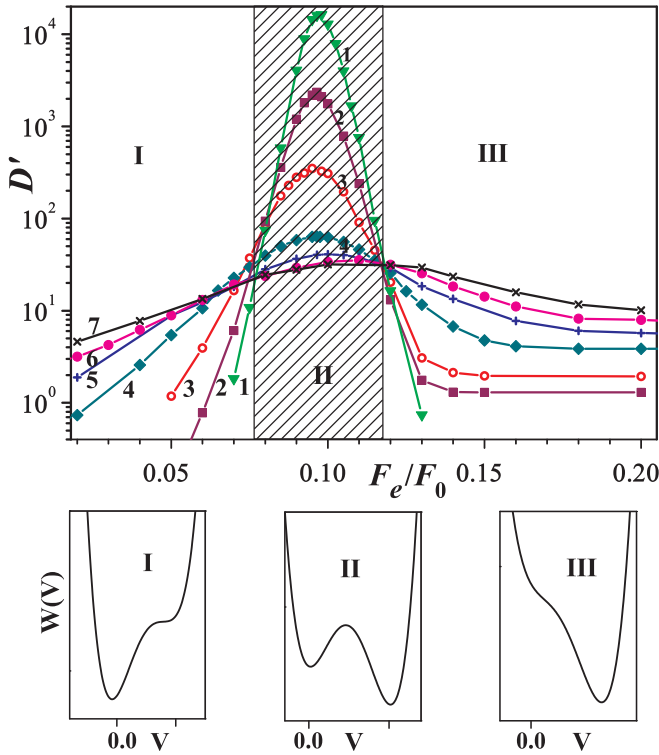


FIG. 1. Dependence of the dimensionless diffusivity on the external constant driving at different temperatures (top). The region of anomalous temperature dependence (II) is hatched. The friction coefficient $\gamma' = 0.2$. 1: $T^\dagger = 0.097$ [$T = 90$ K for the potential characteristic of the H-adatom diffusion on metal surface (6)]; 2: $T^\dagger = 0.129$; 3: $T^\dagger = 0.194$; 4: $T^\dagger = 0.388$; 5: $T^\dagger = 0.582$; 6: $T^\dagger = 0.776$; 7: $T^\dagger = 0.969$. Bottom: the effective velocity potential in the three force regions. Left, middle, and right diagrams correspond to $F_e/F_0 = 0.06, 0.095, \text{ and } 0.25$ respectively.

To understand physical reasons of the abnormal temperature dependence of the diffusivity in these two different (time-periodic, and constant) driving regimes we consider the periodic driving regime in more detail below. For piecewise constant periodic driving one can use intuition gained in the constant driving problem for the time intervals in which F_t stays constant; the findings are thus easier to interpret. Most of the results in this work are for the PCP driving setup.

In [22] it was shown that the transport properties of an ensemble of underdamped particles in a washboard potential can be found by considering simpler overdamped motion in effective potential $W_{F_e}(V)$ in velocity space. The problem thus showed similarities with the problem of active Brownian particle motion [35]. Stationary velocity distribution function $N_W(V) = N_0 \exp(-m^2 W_{F_e}/\gamma k_B T)$ defined $\langle V \rangle(F_e, T)$ and D that agreed well with the direct numerical simulation results for all values of $F \lesssim 0.5 F_0$, temperatures in the range $T^\dagger \in [0.129; 0.776]$, friction $\gamma' \in [0.1; 0.4]$ in the definitions of dimensionless quantities adopted here; Eqs. (10) and (11). The agreement was progressively better at smaller γ' as expected.

For F_e in region II $W_{F_e}(V)$ has two minima, running and locked populations [near corresponding minima of $W_{F_e}(V)$] coexist, mutual motion between these populations with velocity $\approx F_e/\gamma$ is responsible for the enhanced diffusion. In the expression for the diffusivity, $D = \langle \Delta V^2 \rangle \tau_{\text{corl}}$, the correlation

time τ_{corl} factor was shown to be responsible for the main features in $D(F, T)$ dependence, numerically found in [25]. τ_{corl} showed proper nonmonotonic dependence on F , with a maximum near F_{cr} , progressively more pronounced at smaller T . τ_{corl} increased at temperature decreasing $\propto \exp[\mathcal{E}/(k_B T)]$ (for certain $\mathcal{E} > 0$); this increase at low T reflected the Kramers rate for transitions in the double-well velocity potential between the wells corresponding to the locked and running states.

Schematics of the effective velocity potential in the three regions of the applied force are shown in the bottom insets in Fig. 1. These were obtained here as $-\gamma k_B T m^{-2} \ln N(V)$ from the distribution function $N(V)$ found numerically, by binning the results of Monte Carlo simulations of Eqs. (1), (2), and (5) in velocities, for the given $F_t(t) = F_e = \text{const}$. The first inset corresponds to $F_e = 0.06 F_0$, at which only locked solutions exist. In the second inset $F_e = 0.095 F_0$, corresponding to the maximal diffusivity; both types of solutions coexist at this force value. Finally $F_e = 0.25 F_0$ corresponding to region III is shown in the third inset; at this F_e only running solutions are realized at late times. The boundaries between regions I and III depend on γ and m (on γ' in the dimensionless problem). At smaller γ' these boundaries move to the left, to the lower force values, and the width of region II decreases. In the current study we use the same fixed values of γ and m as in [22].

It may be expected that the same picture for different temperature behaviors of the diffusivity, with the analogous three regions I–III of the external force amplitudes, holds for PCP driving, at least at small frequencies Ω . The description with the effective potential is applicable, the potential $W(V)$ keeping constant form for each of the two half periods of the external driving [on which F_t stays constant, this F value defining corresponding $W(V|F, \gamma)$].

Below we show that relating the behavior at periodic driving to such at constant driving is subtle. Similar three regions of the external force amplitudes F_e exist, differing in qualitative $D(T)$ dependence. TAD is realized in regions II and III, for certain finite intervals of the frequencies. At any fixed frequency Ω as the temperature gets lower the dependence $D(T)$ starts progressively deviating from such at constant driving. This is due to the fact that the relaxation time in velocities grows at T decreasing, and on progressively longer parts of the driving half period π/Ω actual distribution $N(V, t)$ differs from stationary (4). At temperatures below a certain critical $T_{\text{TAD}}(\Omega)$ normal temperature dependence of the diffusivity is restored. We demonstrate these features by analyzing $D(T|\Omega)$ in sequence for the above values of F_e ($F_e/F_0 = 0.06, 0.095, 0.25$), that correspond to regions I, II, III in the constant external force problem.

We observe a transient anomalous diffusion phase, and see how its characteristics relate to the diffusivity in the asymptotic late time regime, when normal diffusion sets in. The properties of this anomalous diffusion phase are different in the three regions of the applied force amplitudes; this translates into different functional dependence of the diffusivity on the temperature.

A. Region I: $F_e/F_0 = 0.06$, varying frequency

Here we investigate how the diffusivity changes with (dimensionless) frequency $\omega = \Omega T_0$ of the external driving

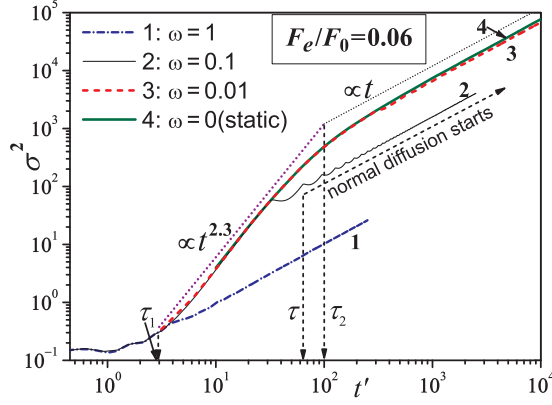


FIG. 2. Time dependence of the dimensionless dispersion for the force value $F_e = 0.06F_0$ (region I) for different force frequencies. τ_2 denotes the time when superdiffusion transitions to normal diffusion at constant driving ($\omega = 0$). $\tau = 2\pi/\omega$ is the period of the external periodic driving. $T^\dagger = 0.194$. 1: $\omega = 1$; 2: $\omega = 10^{-1}$; 3: $\omega = 10^{-2}$; 4: $\omega = 0$ (constant external force). Straight dashed and dotted lines show the power-law fitting behavior of the dispersion.

at the driving amplitude $F_e = 0.06F_0$. We show that the diffusivity stays nearly constant at small frequencies, up to the reciprocal superdiffusion regime time span. At frequencies above this the diffusivity drops according to a power law with an exponent related to the exponent of the superdiffusion. This power-law dependence holds up to frequencies a few times less than Ω_0 . The diffusivity grows with the temperature (normal temperature behavior), related to the superdiffusion regime duration increasing with T .

Figure 2 shows the growth of the particle dispersion with time. At constant external driving this growth demonstrates a clear superdiffusion regime, $\sigma^2 \propto t'^\alpha$, $\alpha > 1$, that switches to normal diffusion (same power-law growth but with $\alpha = 1$) after a certain time τ_2 . τ_2 as well as the superdiffusion exponent α depend on F_e/F_0 and other problem parameters, γ' and T' . For the values used $\tau_2 \approx 100$, $\alpha \approx 2.3$. Lowercase τ 's everywhere are dimensionless, normalized to the period of small oscillations T_0 at the lattice potential minimum at $\gamma' = 0$. σ^2 and D' are dimensionless dispersion and diffusivity.

Curves 1–3 correspond to three different frequencies. Oscillations in $\sigma^2(t')$ are clearly seen with double driving frequency, 2ω . These are particularly large at ω around $\omega_2 = 2\pi/\tau_2$ (curve 2). At these values, interestingly, intervals of $\sigma^2(t)$ decreasing with time are observed. This effect can be seen in earlier works [36].

At frequencies below $\omega_2 = 2\pi/\tau_2$ the curves $\sigma^2(t)$ closely follow that at $\omega = 0$ (constant external force, curve 4). At higher frequencies the superdiffusion phase effectively ends after one period τ of the external force; normal diffusion sets in (in the sense that averaged over the driving period $\langle d(\sigma^2)/dt \rangle_t \approx \text{const}$). Higher frequencies of the driving correspondingly result in lower diffusivity, as the interval of σ^2 growing with time faster than linearly is shorter than at lower frequencies.

These results suggest the following approximations for the average over the driving period dispersion $\overline{\sigma^2(t')}$, valid not too close to the transition moments between different diffusion

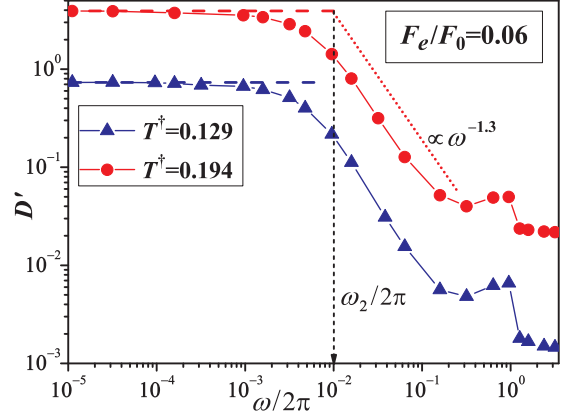


FIG. 3. Dependence of diffusivity D' on the driving frequency at $T^\dagger = 0.129$ (triangles) and 0.194 (circles). The dashed line asymptotes show the diffusivity values at constant driving with the same $F_e/F_0 = 0.06$. The slanting dotted line shows the power-law drop of D' at intermediate ω 's.

regimes:

$$\ln \frac{\overline{\sigma^2}}{\sigma_0^2} = \begin{cases} \approx 0 & \text{at } t' < \tau_1 \\ \alpha \ln(t'/\tau_1) & \text{at } t' \in (\tau_1; \tau_{2,\omega}) \\ \alpha \ln(\tau_{2,\omega}/\tau_1) + \ln(t'/\tau_{2,\omega}) & \text{at } t' > \tau_{2,\omega} \end{cases} \quad (14)$$

Here $\sigma_0^2 = \sigma^2|_{t=0}$ (for the approximately Boltzmannian initial distribution of the particles in $x' \in (-0.5; 0.5)$ well of the potential), $\tau_{2,\omega} = \min(\tau_2, \tau)$; τ_1 is close to the first potential well exit time. Constants are chosen in such a way that the spline approximation (14) is continuous. Quantities α , $\tau_{1,2}$ depend on the problem parameters, T' , F_e/F_0 , and γ' . At fixed values of these parameters, the last approximation yields the dependence of the diffusivity $D' = \lim_{t' \rightarrow \infty} \sigma^2/(2t')$ on the driving period τ ,

$$D'(\tau) = \begin{cases} (1/2)\sigma_0^2\tau_1^{-\alpha}\tau^{\alpha-1} & \text{at } \tau_1 < \tau < \tau_2 \\ (1/2)\sigma_0^2\tau_1^{-\alpha}\tau_2^{\alpha-1} & \text{at } \tau > \tau_2 \end{cases}, \quad (15)$$

or on its frequency $\omega = 2\pi/\tau$,

$$\frac{D'(\omega)}{D'(0)} = \begin{cases} 1 & \text{at } \omega < \omega_2 \\ (\omega/\omega_2)^{1-\alpha} & \text{at } \omega_2 < \omega < 2\pi/\tau_1 \end{cases}. \quad (16)$$

The diffusivity thus should stay about constant at $\omega < \omega_2$, and at the larger driving frequencies drop with ω according to the power law, with exponent equal to $1 - \alpha$, determined by the superdiffusion exponent.

Figure 3 shows simulation results for $D'(\omega)$. Dotted lines show approximations Eq. (16). Dashed lines show the diffusivity at constant driving with the same F_e value. These results confirm the features suggested by Eq. (16), away from transition frequency $\omega_2 = 2\pi/\tau_2$ and up to $\omega/2\pi \approx 0.1$. $D(\omega) < D(0)$ at any ω , and decreases with ω , up to the dimensionless frequency values $\omega/2\pi \approx 0.3$.

Further ramification might have been added in Eqs. (14)–(16) for the case $\tau < \tau_1$, changing τ_1 to $\tau_{1,\omega} = \min(\tau_1, \tau)$; that would indeed lead to $D(\omega)$ increasing at $\omega > 2\pi/\tau_1$. With our parameters, however, resulting approximations are an overstretch; the diffusion gets markedly nonequilibrium at

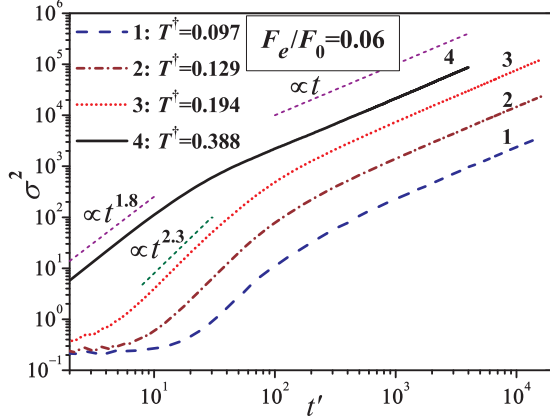


FIG. 4. Dispersion variation with the temperature, at constant driving ($\omega = 0$). 1: $T^\dagger = 0.097$; 2: $T^\dagger = 0.129$; 3: $T^\dagger = 0.194$; 4: $T^\dagger = 0.388$. The short-dashed straight lines show power-law fits for the transient superdiffusion regime, and the late-time normal diffusion.

such high ω 's, resulting in the complex $D(\omega)$ behavior at ω approaching 2π . More on this in Sec. III D.

Finally, Fig. 4 shows $\sigma^2(t)$ for a range of temperatures at constant driving. Despite the superdiffusion exponent α is seen to decrease with the temperature; the time span of the superdiffusion regime $\tau_{\text{spd}} = \tau_2 - \tau_1$ grows fast with the temperature. As a result the dispersion is larger for larger temperatures at any given time. At late times this translates into diffusivity being larger at higher temperatures, so normal (increasing) $D(T)$ dependence is realized at force amplitudes in region I.

B. Region II: $F_e/F_0 = 0.095$

Here we repeat analysis of the previous section for periodic driving with amplitude $F_e = 0.095F_0$ (the value at which the maximal diffusivity is achieved at constant driving). In the same manner as for the driving amplitude in region I, transition from initial superdiffusion phase to normal diffusion at late times is observed, around time τ_2 . At driving frequency ω growing, the diffusivity again decreases only slightly from $D(\omega = 0)$ till ω reaches $\omega_2 = 2\pi/\tau_2$. It decreases fast, according to the same power law $D(\omega)/D(0) = (\omega/\omega_2)^{1-\alpha}$, at larger ω 's, up to $1/\tau \approx 0.1$. Contrary to the case of weaker driving considered in the previous section, superdiffusion duration $\tau_{\text{spd}} = \tau_2 - \tau_1$ now *decreases* with the temperature. This leads to diffusivity growing at temperature decrease (TAD), at moderately low frequencies. This is the main effect we intended to find in the periodic driving setup, extending our previous findings at constant driving [22].

Figure 5 shows the growth of the particle dispersion with time. Again the interval of superdiffusion is observed, and it ends after one period of PCP driving or after τ_2 (the end time of superdiffusion at constant driving), whichever is smaller. Thus the same approximations, Eqs. (14)–(16), are applicable for the (averaged over τ) dispersion growth $\sigma^2(t')$ and dependence of the diffusivity on the driving frequency $D'(\omega)$. Simulation results for $D'(\omega)$, Fig. 6, again agree with prediction, Eq. (16).

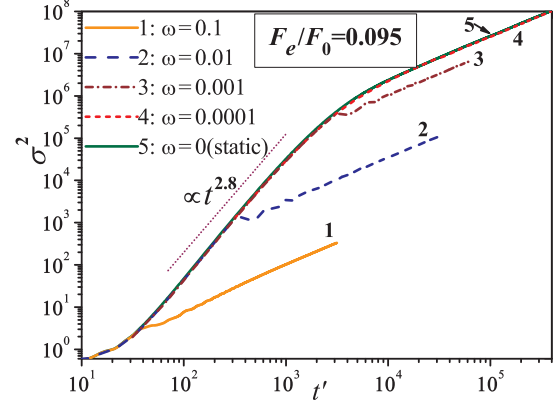


FIG. 5. Time dependence of the dimensionless dispersion for the force value $F_e = 0.095F_0$ (region II) for different force frequencies. Curves 1–5, bottom to top: (dimensionless) $\omega = 10^{-1}$, 10^{-2} , 10^{-3} , 10^{-4} , 0 (constant driving). $T^\dagger = 0.194$.

As $D(\omega)$ does not vary much at $\omega < \omega_2$, TAD must be observed at small frequencies, at it is observed at constant driving [[22]: $D(F_e, \omega = 0)$ decreases with the temperature when F_e is in region II]. Such an abnormal dependence on the temperature is due to longer jumps the particles perform on average at lower temperatures. This in turn follows from lower probability at lower temperatures to turn the running particle into a locked state: such a transition requires certain threshold energy transfer to such a particle, and at lower temperatures the probability of such a transfer decreases as an exponential of inverse temperature. Hence the running particle travels at about the stationary speed F_e/γ (the speed fluctuating around this average due to the lattice potential) for increasingly longer distances before getting trapped again in some next well of the potential, resulting in larger diffusivity at smaller temperatures. This mechanism is not applicable in region I, where only locked solutions are realized.

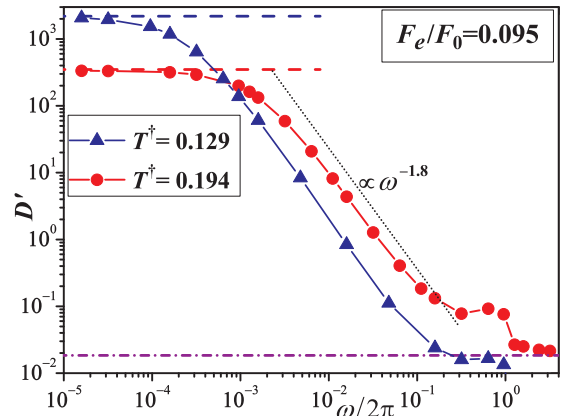


FIG. 6. Dependence of diffusivity D' on the external force frequency ω , at $T^\dagger = 0.129$ (triangles) and 0.194 (circles). The dashed line asymptotes show the diffusivity values for constant driving with the same $F_e/F_0 = 0.095$. Dotted line shows the power-law drop of D' at higher ω 's. The dot-dashed horizontal line asymptote (for high ω) is at the diffusivity value in the lattice periodic potential in the absence of extra driving, $F_t(t) = 0$, for $T^\dagger = 0.194$.

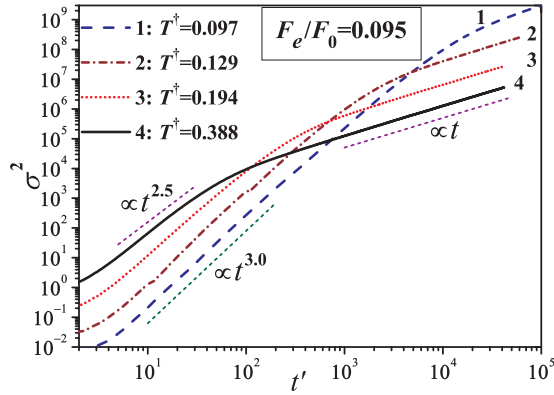


FIG. 7. The dispersion variation with the temperature, at constant driving ($\omega = 0$). 1: $T^\dagger = 0.097$; 2: $T^\dagger = 0.129$; 3: $T^\dagger = 0.194$; 4: $T^\dagger = 0.388$. $F_e/F_0 = 0.095$.

In terms of the dispersion evolution features, this phenomenon of the diffusivity growing at the temperature decreasing results from the superdiffusion duration $\tau_{\text{spd}} = \tau_2 - \tau_1$ growing at temperature decreasing, as Fig. 7 demonstrates. This qualitatively differs from the situation at driving amplitude in region I (end of the previous section). We note that α increases with the temperature decreasing, the same as in region I.

At higher frequencies, on the other hand, the diffusivity starts increasing with the temperature (normal behavior). This results from τ_2 decreasing with the temperature, as can be seen in Fig. 7. Despite that $D(\omega = 0)$ is larger at smaller temperature T_1 , as ω grows the $D(\omega|T_1)$ starts decreasing according to the power law earlier [at ω 's near the smaller $\omega_2 = 2\pi/\tau_2(T_1)$] than $D(\omega|T_2)$ for $T_2 > T_1$ does. And the exponent of this power law decreases with T decreasing, $1 - \alpha(T_1) < 1 - \alpha(T_2) < 0$ —therefore at larger frequencies, commensurate with ω_2 , the diffusivity starts increasing with the temperature, and TAD disappears.

As is the case for the driving amplitude in region I, $D(\omega)$ decreases monotonically with ω from $D(0)$, up to the frequency values $\omega \approx 0.3 \times 2\pi$. At frequencies that high the particle transport becomes substantially nonequilibrium, affecting the functional dependence $D(\omega)$, as discussed in Sec. III D below.

C. Region III: $F_e/F_0 = 0.25$

For strong driving (region III, in which the diffusivity decreases with F_e in the constant driving setup, and increases with the temperature) we demonstrate in this subsection that the dependence of the dispersion on time shows extra features. After the initial phase of superdiffusion at times $t' < \tau_2$, long-lasting dispersionless regime sets in, till $\tau_3 \sim 10^3 \tau_2$. In this phase the dispersion stays nearly constant. As at the weaker external driving (regions I and II), both of these anomalous diffusion regimes may be interrupted earlier in the case of high driving frequency, after about a period of the driving. At late times normal diffusion sets in. Dependence $D(\omega)$ is nonmonotonic here, agreeing with findings in [30]. D reaches a maximum near $\omega = \omega_2 \equiv 2\pi/\tau_2$. TAD is observed at intermediate frequencies.

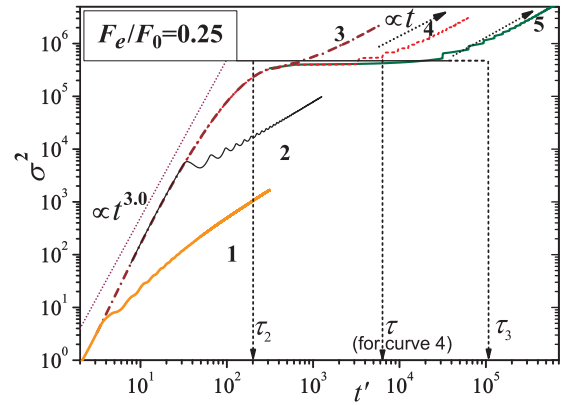


FIG. 8. Time dependence of the dimensionless dispersion at $F_e = 0.25 F_0$ (region III) for different force frequencies. Curves 1–5: (dimensionless) $\omega = 1, 10^{-1}, 10^{-2}, 10^{-3}, 10^{-4}$. $T^\dagger = 0.194$. Dotted lines show power-law fitting behavior of the dispersion.

Figure 8 shows the particle dispersion as a function of time. At low frequencies of the driving, superdiffusion is observed till $\tau_2 \approx 200$. A dispersionless regime is realized later, at $t' \in (\tau_2; \tau_3)$. Physically τ_2 is the time at which the particle distribution function in velocities assumes its stationary form. The distribution in space is still strongly nonequilibrium at τ_2 ; it has exponential tail and sharp front [16] (in the direction of F). It takes till τ_3 for the distribution function to assume an approximately Gaussian shape in space (if averaged over the potential spatial period). On the interval $(\tau_2; \tau_3)$ the dispersion does not increase substantially. After τ_3 normal diffusion sets in, $\sigma^2 = 2D't' + o(t')$ at $\tau_3 \ll t' \rightarrow \infty$.

The whole curve $\sigma^2(t')$ differs insignificantly from $\sigma^2(t')$ in constant driving setup if the driving frequency $\omega < \omega_3 \equiv 2\pi/\tau_3$. This $\sigma^2(t')$ dependence is modified at higher frequencies of the external driving (in a similar way to the behavior discussed in Secs. III A and III B at weaker driving). For $\omega \in (\omega_3; \omega_2)$ the dispersionless regime is interrupted after about one period of external force, after which time approximately linear dependence (if averaged over times $\sim 2\pi/\omega$) sets in, $\langle d\sigma^2/dt' \rangle_{t'} = 2D'$, D' equal to its asymptotic (at $t' \rightarrow \infty$) value. At yet higher driving frequencies, $\omega > \omega_2$, the dispersionless regime is not realized at all; normal diffusion sets in right after the prematurely interrupted interval of superdiffusion.

Similarly to the previous sections, the described above dependence of $\ln \overline{\sigma^2}$ on $\ln t'$ can be schematized by the following continuous piecewise linear approximation (meaningful not too close to switching time points τ_{1-3}):

$$\ln \frac{\overline{\sigma^2}}{\sigma_0^2} = \begin{cases} \approx 0 & \text{at } t' < \tau_1 \\ \alpha \ln(t'/\tau_1) & \text{at } t' \in (\tau_1; \tau_{2,\omega}) \\ \alpha \ln(\tau_{2,\omega}/\tau_1) & \text{at } t' \in (\tau_{2,\omega}; \tau_{3,\omega}) \\ \alpha \ln(\tau_{2,\omega}/\tau_1) + \ln(t'/\tau_{3,\omega}) & \text{at } t' > \tau_{3,\omega} \end{cases} \quad (17)$$

Here $\tau_{3,\omega} = \min(\tau_3, \tau)$, $\tau_{2,\omega} = \min(\tau_2, \tau)$; $\tau > \tau_1$ is assumed. As before, $D(\omega)$ can be found from this, showing the same power-law decay as in Eq. (16) at $\omega > \omega_2$, and an additional,

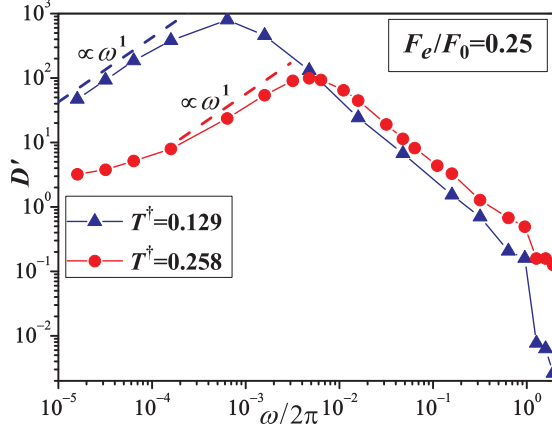


FIG. 9. Dependence of the dimensionless diffusivity D' on the driving frequency, at $T^\dagger = 0.129$ (triangles) and 0.258 (circles). The dashed lines show approximately linear growth at $\omega \in (\omega_2; \omega_3)$.

linearly growing with ω feature at intermediate frequencies:

$$\frac{D(\omega)}{D(0)} = \begin{cases} 1 & \text{at } \omega < \omega_3 \\ \omega/\omega_3 & \text{at } \omega \in (\omega_3; \omega_2). \\ (\omega/\omega_2)^{1-\alpha} \omega_2/\omega_3 & \text{at } \omega > \omega_2 \end{cases} \quad (18)$$

Simulation results for $D(\omega)$ are shown in Fig. 9 for two temperatures. They indeed show the features suggested in Eq. (18). At high frequencies, $\omega > \omega_2$, the superdiffusion phase switches to normal diffusion earlier than at τ_2 , at time $\sim \tau = 2\pi/\omega$. This behavior is the same as for the driving amplitude in regions I and II. Thus in the same manner the diffusivity grows as ω decreases, as the longer interval (till $t' \approx \tau$) of superdiffusive dispersion growth is used at the driving period τ getting longer. However at smaller frequencies, $\omega_3 < \omega < \omega_2$, it is the dispersionless phase that gets interrupted prematurely (i.e., it is not realized in full, till τ_3 , as it would have at $\omega = 0$), so the earlier such a switch occurs (i.e., the shorter the τ), the larger the diffusivity obtained in the late-time normal diffusion regime. This explains the growth of $D(\omega)$ with ω at $\omega \in (\omega_3; \omega_2)$. The maximum in $D(\omega)$ is thus observed, at $\omega_{\max} \approx \omega_2$.

This differs from monotonically decreasing $D(\omega)$ in regions I and II. Such a nonmonotonic dependence $D(\omega)$ was observed in [30,31]; the driving studied was sinusoidal in time, its amplitude (indeed) corresponded to region III in the terminology of this work.

ω_{\max} together with $2\pi/\tau_2$ increase with the temperature. The maximal value of the diffusivity (achieved at ω_{\max}) increases as the temperature decreases, due to the dispersionless phase duration $\tau_3 - \tau_2$ growing fast at temperature decreasing. And so does $D(\omega)$ at a given ω near ω_2 in a limited range of temperatures. So abnormal temperature dependence of the diffusivity (TAD) is realized in the intermediate region of the driving frequencies around ω_2 . The temperature dependence of the diffusivity is studied in more detail in Sec. IV below.

D. Diffusivity at high driving frequency ω

As the simulation results suggest, the power-law decay of $D(\omega)$ at large ω 's (Figs. 3, 6, and 9) does not hold at

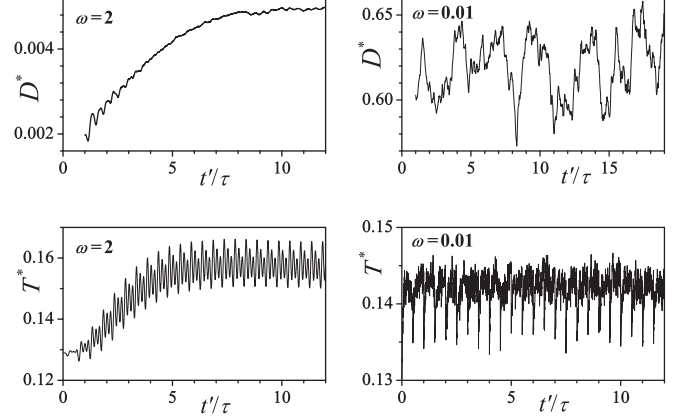


FIG. 10. Evolution of the diffusivity and the kinetic temperature for high and small frequencies of the driving, $\omega = 2$ and 10^{-2} . $F_e/F_0 = 0.06$. Note that time normalized to one driving period τ (rather than to \mathcal{T}_0 as in the previous t -dependence graphs) is shown along the abscissa axis.

frequencies that are too high, above $\sim 1/10$ th of the frequency of small oscillations at the lattice potential minima. This is due to the diffusion process becoming markedly nonequilibrium. The interval π/ω between $F_i(t)$ sign switching is too short for $N(V; t)$ to relax to its equilibrium form (4) by the end of each driving half period. The distribution function in velocities differs significantly from such at constant driving at all times; a description in terms of the velocity potential $W(V)$ is no longer useful.

To analyze this we introduce kinetic temperature $T^* = m\langle \Delta v^2 \rangle / U_0$ (i.e., made dimensionless with the same multiplier k_B/U_0 as T^\dagger), and study its evolution at different ω 's; Fig. 10, bottom. At low frequency, T^* does not change (only shows random noise) after one period $\tau = 2\pi/\omega$ of the driving. At larger $\omega = 2$ regular oscillations in T^* are observed at all times, with amplitude of order 5% of the average T^* value. That average is about 10% higher than the average T^* at $\omega = 10^{-2}$. T^* averaged over the driving oscillation period grows for about $t'_{\text{st}} \approx 7\tau$ until it reaches its stationary value.

Together with T^* , $\sigma^2(t')$ also shows transient behavior at $t' < 7\tau$. We illustrate this in the top graphs in Fig. 10, by plotting

$$D^*(t') = [\sigma^2(t' + \tau) - \sigma^2(t')]/(2\tau). \quad (19)$$

In settled “normal diffusion” regime this quantity must coincide (in average over the driving period of duration τ) with the diffusivity, as in such a regime theoretically $\sigma^2(t + n\tau) = \sigma^2(t) + n\sigma^2(\tau)$ for $n \in \mathbb{N}$.

These results in part mean that the rule of superdiffusion or dispersionless phase (however these are modified in the high-frequency regime) terminating and turning into normal diffusion after one period of the driving no longer applies at high driving frequencies. This leads to the $D(\omega)$ derivation based on approximations Eqs. (14) and (17) progressively less accurate at higher ω 's, the power-law decay first slowing down, and then going into a completely different regime at ω approaching 2π .

At $\omega > 2\pi$ the diffusivity tends to the diffusivity of particles in the lattice periodic potential in the absence of extra driving

$F_i(t)$. Such an asymptote is shown by the horizontal dot-dashed line in Fig. 6.

IV. DEPENDENCE OF DIFFUSIVITY ON TEMPERATURE AT FIXED DRIVING FREQUENCY

Having studied how the temperature behavior of diffusion changes at gradual driving frequency increase, here we investigate in more detail how the diffusivity changes with the temperature at fixed frequency. Besides theoretical importance, the results are of interest to experimentalists. Oftentimes changing the frequency in the system is problematic, while changing the temperatures is simpler; so the findings in this section are more straightforward to test.

The left part of Fig. 11 shows how the diffusivity changes with T^\dagger at fixed $\omega = 10^{-2}$. For the driving amplitude in region I (filled circles in Fig. 11) the diffusivity monotonically grows with the temperature, this (normal) behavior agreeing with such at constant driving [22]. For F_e in regions II and III TAD is observed, as already noted in Secs. III B and III C. TAD is confined to limited (from below) temperature intervals, contrary to the TAD behavior observed in [22] for constant driving. In [22] the diffusivity was numerically checked growing (only in region II at $\omega = 0$) at temperature decreasing down to $T^\dagger = 0.097$. Such a behavior was understood theoretically, dependence $D \propto \exp[\mathcal{E}/(k_B T)]$ was predicted at low temperatures going all the way down to 0, and agreed well with simulation results.

In the current setup with periodic driving, similar temperature dependence is observed too,

$$D \propto \exp(\epsilon_1/T^\dagger), \quad \epsilon_1 > 0, \quad (20)$$

but only above certain temperature. The growth slows down as the temperature keeps decreasing. D reaches maximum $D_{\max}(T_{\max})$ at certain T_{\max} , and starts decreasing with further decrease in T . The behavior at lower temperatures is well

approximated by

$$D \propto \exp(-\epsilon_2/T^\dagger), \quad \epsilon_2 > 0. \quad (21)$$

In the absence of driving we observe $\epsilon_2 = 1$ (corresponding dimensionful quantity $\mathcal{E}_2 = U_0$)—classical Arrhenius temperature behavior of the diffusivity. ϵ_2 decreases with F_e , whereas ϵ_1 increases. T_{\max} and D_{\max} increase with F_e as well.

The temperature behavior of the diffusivity can be understood from its relation, Eqs. (15)–(17), with times τ_{1-3} characterizing transient diffusion regimes of the system. Considered at fixed ω this connects the temperature dependence of the diffusivity to the $\tau_{1-3}(T)$ dependence in a graphic way, Fig. 12. $\tau_{1-3}(T)$ may be found by studying the particle dispersion evolution with time at different T and constant in time driving F_e . The temperature dependence is different for F_e in regions I–III.

For driving F_e in region I, τ_1 (the time at which superdiffusion starts, about the potential well escape time) increases with the temperature decreasing. $\tau_{\text{spd}} = \tau_2 - \tau_1$ at the same time decreases. This is seen to result in the diffusivity growing with the temperature, agreeing with the results shown in the left ($\omega = 10^{-2}$) part of Fig. 11.

In region II τ_1 increases with the temperature decreasing as well. τ_{spd} however also increases with the temperature decreasing (middle graph in Fig. 12, curves 3–5)—contrary to the behavior at F_e in region I. As a result TAD is realized at these temperatures. Graphically, in Fig. 12 (the middle plot) curves corresponding to the higher temperatures are above those for the lower temperatures at early times, in the superdiffusion regime, the same situation as for F_e in region I. However due to the shorter τ_{spd} they transition into the normal (growing with time slower) diffusion regime earlier than the curves for lower T . Consequently σ^2 becomes smaller at late enough times for the higher temperature system, translating to the smaller diffusivity.

At temperature $T_{\max}(F, \omega)$ ($T^\dagger \approx 0.194$ in this graph) τ_2 becomes equal to $\tau = 2\pi/\omega$, the period of the driving. At this temperature the maximal diffusivity is achieved, corresponding to the longest actual superdiffusion regime time span at the given driving frequency. TAD is only realized at the temperatures above $T_{\max}(F_e, \omega)$. Indeed, even though τ_{spd} (superdiffusion duration at constant driving) still grows at further temperature decrease together with τ_2 , in the periodic driving setup superdiffusion effectively ends earlier, at $t' \approx \tau$. It is this superdiffusion interruption at $t' \approx \tau$ that makes $D(T)$ behavior at lower temperatures diverge in the periodic driving setup from that at constant driving. In the constant driving problem, based on the same logic, TAD must be realized all the way down to $T = 0$; in agreement with conclusions in [22].

It is clear from this argument that there is no uniform convergence with ω of $D(T)|_\omega$ curves to $D(T)|_{F=\text{const}}$. As ω gets smaller $D(T)|_\omega$ does get close to the limit $D(T)|_{\omega=0}$ curve on a longer T interval, down to progressively lower temperatures. However at any ω there exists $T_{\text{TAD}}(\omega)$ such that the normal temperature dependence of the diffusivity is restored at $T < T_{\text{TAD}}(\omega)$. This nonuniform convergence is shown in the right plot in Fig. 11.

The same behavior is observed in region III. The maximal diffusivity is achieved at $T_{\max}(F_e, \omega)$ corresponding to the longest superdiffusion regime duration at the given ω . The

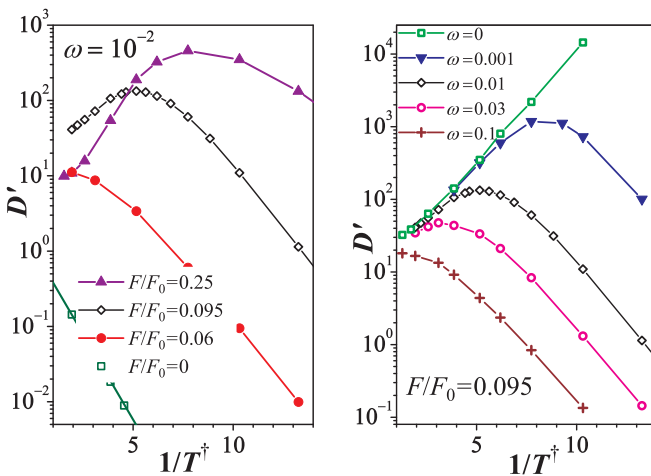


FIG. 11. Dimensionless diffusivity vs $1/T$ at left: $\omega = 10^{-2}$, force amplitudes $F_e/F_0 = 0$ (squares, and linear fit), 0.06 (circles), 0.095 (diamonds), 0.25 (triangles); right: $F_e/F_0 = 0.095$, top to bottom, $\omega = 0$ (squares), 10^{-3} (triangles), 10^{-2} (diamonds), 3×10^{-2} (circles), 10^{-1} (pluses).

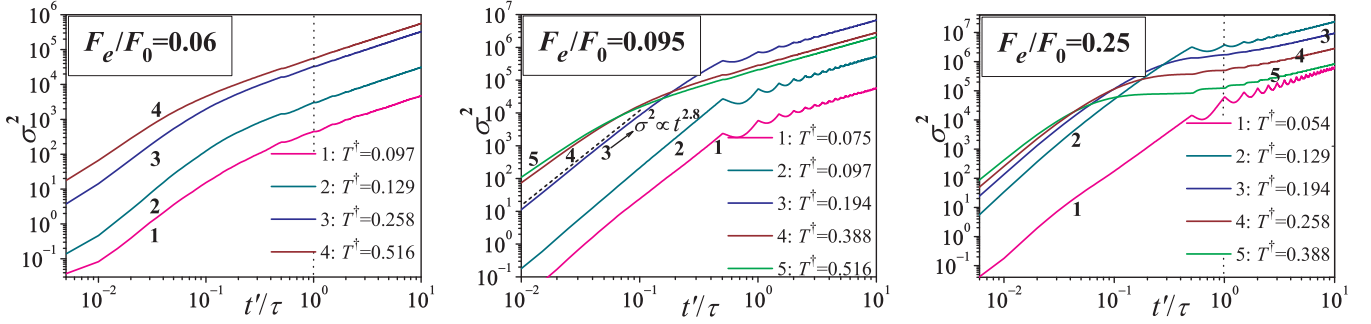


FIG. 12. Dispersion of the particles as a function of time at different temperatures. Force amplitudes in regions I–III. $\omega = 10^{-2}$.

lowest temperature at which TAD is realized is the one at which τ_2 reaches the period of external force τ (more precisely, the time of superdiffusion interruption at a given ω). At this temperature $\partial D/\partial T|_{\{F_e, \omega\}=\text{const}}$ crosses zero value. The interval of temperatures, in which TAD is observed, is wider than that at the driving in region II, due to the presence of dispersionless phase (curve 4 in the right plot in Fig. 12). Experimentally it is simpler to observe TAD at larger F_e , at which within the period of $F_t(t)$ the superdiffusion regime duration is used to a larger extent, and the temperature interval of TAD is thus wider.

Presented results on the diffusion under external driving can be summarized by the following schematics, Fig. 13. Force amplitudes fall into three regions, I–III. In region I the diffusivity grows with the temperature increasing. In regions II and III the dependence $D(T)$ is nonmonotonic; it shows a maximum at certain T_{\max} . Below T_{\max} the temperature dependence of the diffusivity is normal, $\partial D/\partial T > 0$. The temperature interval of TAD exists above T_{\max} , $\partial D/\partial T < 0$.

In the driving frequency dependence of the diffusivity, on the other hand, it is regions I and II that look alike: at the frequency decreasing from about $0.3 \times 2\pi$ (in dimensionless units) the diffusivity grows monotonically, getting to a flat region at $\omega < \omega_2$, in which it virtually reaches its limiting $D(\omega = 0)$ value. In region III the $D(\omega)$ curve passes through a maximum, near $\omega = \omega_2 \equiv 2\pi/\tau_2$, corresponding to the termination time τ_2 of the superdiffusion regime at constant driving. At the frequencies getting smaller, the driving period contains a progressively longer interval of the “would-be” (in the constant driving problem) dispersionless and (at yet smaller frequencies) normal-diffusion time interval, resulting in D decreasing at such further ω decrease.

V. SINUSOIDAL IN TIME EXTERNAL DRIVING

Here we show the frequency dependence of the diffusivity for sinusoidal in time external driving. We observe the same features in $D(\omega)$ as we saw for PCP driving. The main

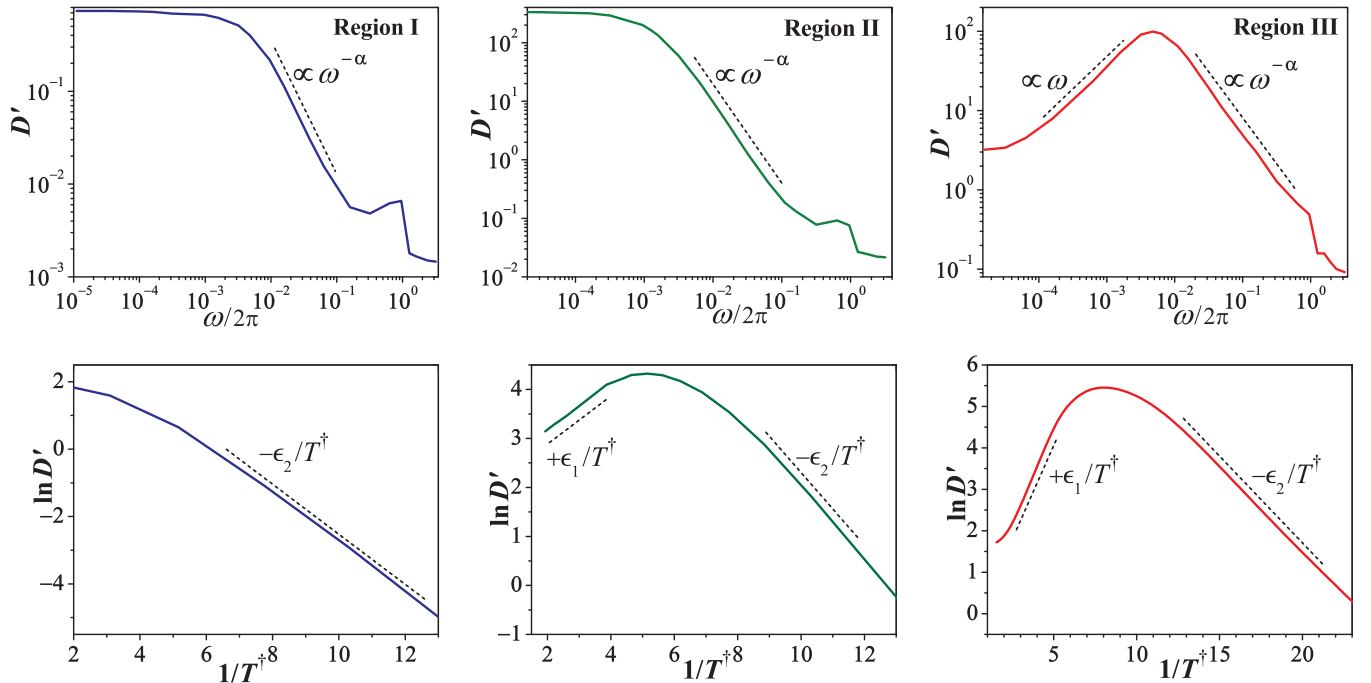


FIG. 13. Features of the dependence of the diffusivity on the driving frequency at fixed temperature (top) and on the inverse temperature at fixed frequency (bottom), for F_e in regions I–III.

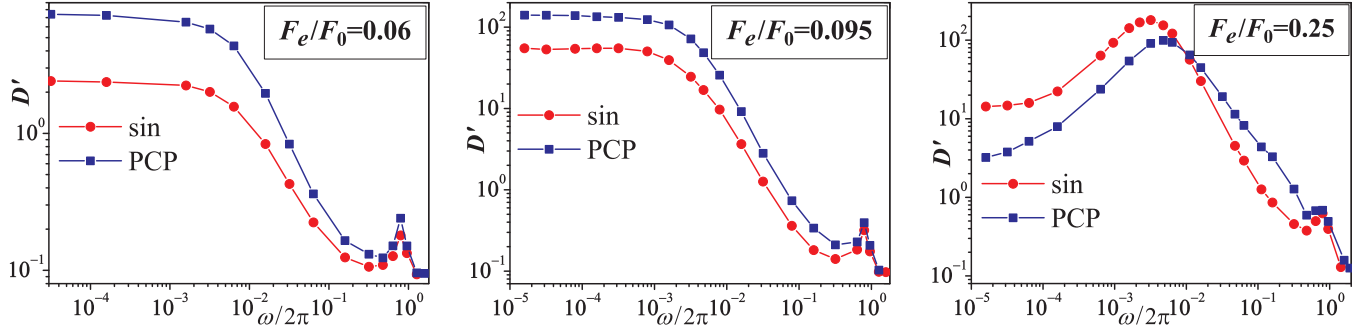


FIG. 14. $D'(\omega)$ for force amplitude in regions I–III. $T^\dagger = 0.258$. Sinusoidal in time (circles) and PCP (squares) driving.

conclusions of the sections above thus appear not to depend critically on the specific form of time dependence of the (smooth enough, symmetric) driving.

Figure 14 presents a comparison between diffusivities at sinusoidal in time and PCP driving. At small frequencies the diffusivity stays close to its value at $\omega = 0$. In regions I and II of the external driving amplitude $D(\omega)$ starts decaying according to a power law at $\omega > 2\pi/\tau_2$, τ_2 being the superdiffusion regime termination time at constant external driving with the same amplitude F_e . In region III $D(\omega)$ grows linearly with ω at intermediate ω 's, reaches a maximum, then shows a power-law decay at larger frequencies. For all force amplitudes the power-law decay switches to more complex behavior at ω reaching a value of about $2\pi/10$.

The presence of periodic driving of any form of time dependence leads to significant enhancement in the diffusivity. This enhancement is somewhat smaller for sinusoidal driving in regions I and II (which can be understood, as at the same F_e the average over period driving $\langle |F_t| \rangle_t$ is smaller for sinusoidal than for PCP driving). In region III the maximum in diffusivity is achieved at smaller ω_{\max} ; the value of D_{\max} is larger than such a maximal diffusivity at corresponding $\omega_{\max, \text{PCP}}$ under PCP driving with the same amplitude F_e . This can be understood from the same argument, as in region III the diffusivity *decreases* with the driving increasing, all other parameters kept constant.

VI. CONCLUSIONS AND DISCUSSION

We investigated enhancement of diffusion in 1D space-periodic underdamped systems by external time-periodic fields. We showed that the diffusion can be enhanced by orders of magnitude at a certain choice of temperatures T , driving amplitudes F_e , and frequencies ω . Three regions of F_e exist, I–III, in which dependencies of diffusivity D on T and ω differ qualitatively.

At all F_e there is an interval of small frequencies, in which D depends only weakly on the frequency, approaching the limiting value $D(\omega = 0)$. This value coincides with D at constant bias force with the same value F_e in the case of piecewise constant in time-periodic (PCP) driving, the form $F_t(t)$ of the driving we focused on in this study. At larger frequencies, from $\omega_2 = 2\pi/\tau_2$ corresponding to the superdiffusion regime termination time τ_2 to about $2\pi/10$, $D(\Omega)$ decays with Ω according to a power law. The exponent of this decay is related to the superdiffusion regime exponent

α . At yet larger frequencies nonequilibrium effects slow down the power-law decay of $D(\Omega)$. After a local maximum in $D(\Omega)$ near $\Omega \approx 0.8\Omega_0$, D tends to its asymptotic value coinciding with the diffusivity in the absence of external driving.

At small driving amplitudes, in regions I and II, $D(\Omega)$ decreases monotonically with frequency Ω from its value at constant driving, all the way till the nonequilibrium effects become critical, at $\Omega \approx 0.3\Omega_0$. At stronger driving, region III, $D(\omega)$ is nonmonotonic, a maximum is reached at $\omega_{\max} \approx \omega_2$. $D(\omega)$ grows monotonically on $\omega \in (0; \omega_{\max})$, this growth is approximately linear on a certain interval to the left of ω_2 .

We studied the temperature dependence of the diffusivity at fixed ω . Contrary to the constant driving problem [22] the diffusivity increases with the temperature for all F_e when the temperature is below a certain frequency-dependent threshold value. Limited temperature intervals exist for the force amplitudes in regions II and III, in which the diffusivity decreases with the temperature [temperature-abnormal diffusivity (TAD)].

The physical reason behind the strong diffusivity enhancement is emergence of two populations of particles under the action of external force, locked and running ones. At optimal F_e and T the number of particles in the two populations is comparable, long flights of the running particles relative to the locked population take place with significant probability, resulting in giant enhancement of diffusion.

For comparison we studied diffusivity under sinusoidal in time driving. We saw that the same features in $D(\omega)$ are observed in the three regions of force amplitudes as in the PCP driving case. We thus conjecture that the qualitative features of $D(\omega, T, F_e)$ behavior are insensitive to specific functional dependence of the (symmetric, smooth enough in t) external force on time.

Periodic driving may be applied in many ways in a number of spatially periodic underdamped physical systems. The region of TAD, enhanced diffusion with abnormal temperature dependence, must exist for such systems. Diffusion of atoms and clusters on solid body surface under the action of microwave radiation is one natural arena for experimental verification and application of the results of the present study. Characteristic oscillation decay time of adatoms varies typically between 10^1 and 10^3 oscillation periods [37]. With the parameters used as an example in the present paper, $U_0 = 80$ meV, $a = 2$ Å (Sec. II A; typical for hydrogen adatoms migrating on a platinum surface), relevant temperatures are $T = T^\dagger U_0/k_B \sim 280$ K (for T^\dagger chosen at 0.3

value), readily accessible experimentally. $\Omega_0/(2\pi) = 1/\mathcal{T}_0 = (2m_H/U_0)^{-1/2}a^{-1} \approx 10^{13} \text{ s}^{-1}$ [cf. Eq. (10)]. For the value of $\gamma' = 0.2$ adopted in this paper, region III corresponds to $F_e/F_0 \gtrsim 0.12$, while region II starts at $F_e \approx 0.08F_0$. Such driving amplitudes can be safely realized and explored, without causing noticeable desorption.

TAD must be observed for the driving frequencies ranging from zero up to approximately $\Omega_2 = \omega_2/\mathcal{T}_0$, of order $1/100$ th of the oscillation frequency of the adsorbate on the substrate at chosen $\gamma' = 0.2$, i.e., $\sim 10^{11} \text{ s}^{-1}$. The upper temperature bound of TAD depends on the potential well depth, and varies for typical adsorbates and substrates in the (100 K; 2000 K) range [38].

One setup to study TAD is in propagation of magnetic particles on nonmagnetic substrate, acted upon with electromagnetic fields. Abnormal diffusion enhancement could be manifested in, e.g., enhanced growth of islands of a new phase at decreasing temperatures.

By drastically enhancing diffusivity in specific direction (along the applied periodic driving) one can manufacture structures of desired geometry on the surface of semiconductors, and on graphene [39,40]. Similarly, periodic driving can be applied in buffer-layer-assisted growth (BLAG) technique [41], in which atoms are initially deposited onto a buffer layer of inert gas on the designated substrate, providing means to create metallic nanowires of designed length and cross section. The same approach may be exercised to affect diffusive mobility of atoms on nanotubes [42] and graphene nanoribbons [43].

Volume diffusion of interstitial atoms and molecules [1,44] is another stage for observing TAD. Ultrasound may be employed for the driving [27], as TAD is manifested at arbitrarily

low frequency (at the driving amplitude in region II). This way one can, for instance, stimulate hydrogen desorption in hydrogen energetics applications [45].

Systems that have become traditional for experimental testing of results of theoretical investigations into variations of Eq. (1), such as Josephson tunnel junctions or diffusion of cold atoms in optical lattices [46], also provide a good playground for verifying the findings of the present work experimentally. On the other hand, findings of the present work can provide useful additional diagnostics for more controversial spatially periodic systems. For instance, complex electron dynamics in arrays of quantum dots [47] results in a yet poorly understood hysteresis loop in current-voltage diagrams, associated with the transition between the insulating and conducting states. Studying the response of the system with the time-periodic source drain bias used might shed light on underlying physics and its characteristic time scales.

Once verified experimentally, the effect of abnormal diffusion enhancement can find applications in a number of new technologies: in sorting of particles, manufacturing surface structures with required properties, controlling penetration of particles through biological and artificial membranes, in memristors, devices with charge density waves, etc.

ACKNOWLEDGMENTS

We are grateful to A. Chechkin for useful discussions. The work of A.V.Z. was supported by the World Premier International Research Center Initiative (WPI Initiative), MEXT, Japan, and JSPS KAKENHI Grant No. JP16H02168.

-
- [1] H. Mehrer, *Diffusion in Solids* (Springer, Berlin, 2007).
- [2] G. Antczak and G. Ehrlich, *Surface Diffusion* (Cambridge University Press, Cambridge, England, 2010); *Molecular Machines Involved in Protein Transport Across Cellular Membranes, The Enzymes Vol. XXV*, edited by R. Dalbey, C. Koehler, and F. Tamanoi (Elsevier, Amsterdam, 2007); *Microfluidics and Microfabrication*, edited by S. Chakraborty (Springer, New York, 2010).
- [3] O. M. Braun and Yu. S. Kivshar, *Phys. Rep.* **306**, 1 (1998); C. Dalle-Ferrier, M. Krüger, R. D. L. Hanes, S. Walta, M. C. Jenkins, and S. U. Egelhaaf, *Soft Matter* **7**, 2064 (2011); I. Goychuk, *Beilstein J. Nanotechnol.* **7**, 328 (2016); F. Höfling and T. Franosch, *Rep. Prog. Phys.* **76**, 046602 (2013).
- [4] P. Hänggi and F. Marchesoni, *Rev. Mod. Phys.* **81**, 387 (2009).
- [5] F. Evers, R. D. L. Hanes, C. Zunke, R. F. Capellmann, J. Bewerunge, C. Dalle-Ferrier, M. C. Jenkins, I. Ladadwa, A. Heuer, R. Castañeda-Priego, and S. U. Egelhaaf, *Eur. Phys. J.: Spec. Top.* **222**, 2995 (2013).
- [6] H. Risken, *The Fokker-Planck Equation. Methods of Solution and Applications* (Springer, New York, 1989).
- [7] S.-H. Lee and D. G. Grier, *Phys. Rev. Lett.* **96**, 190601 (2006).
- [8] P. Tierno, P. Reimann, T. H. Johansen, and F. Sagués, *Phys. Rev. Lett.* **105**, 230602 (2010).
- [9] P. Eshuis, K. van der Weele, D. Lohse, and D. van der Meer, *Phys. Rev. Lett.* **104**, 248001 (2010).
- [10] S. Pagliara, C. Schwall, and U. F. Keyser, *Adv. Mater.* **25**, 844 (2013).
- [11] P. Sajeesh and A. K. Sen, *Microfluid. Nanofluid.* **17**, 1 (2013).
- [12] H. D. Vollmer and H. Risken, *Z. Phys. B: Condens. Matter* **34**, 313 (1979); H. Risken and H. D. Vollmer, *ibid.* **33**, 297 (1979).
- [13] H. Risken and H. D. Vollmer, *Phys. Lett. A* **69**, 387 (1979); *Z. Phys. B: Condens. Matter* **35**, 177 (1979); H. D. Vollmer and H. Risken, *ibid.* **37**, 343 (1980); P. Jung and H. Risken, *ibid.* **54**, 357 (1984).
- [14] G. Costantini and F. Marchesoni, *Europhys. Lett.* **48**, 491 (1999).
- [15] H. Gang, A. Daffertshofer, and H. Haken, *Phys. Rev. Lett.* **76**, 4874 (1996); M. Borromeo, G. Costantini, and F. Marchesoni, *ibid.* **82**, 2820 (1999).
- [16] K. Lindenberg, J. M. Sancho, A. M. Lacasta, and I. M. Sokolov, *Phys. Rev. Lett.* **98**, 020602 (2007).
- [17] M. Khoury, J. P. Gleeson, J. M. Sancho, A. M. Lacasta, and K. Lindenberg, *Phys. Rev. E* **80**, 021123 (2009); J. M. Sancho, A. M. Lacasta, K. Lindenberg, I. M. Sokolov, and A. H. Romero, *Phys. Rev. Lett.* **92**, 250601 (2004).
- [18] K. Lindenberg, A. M. Lacasta, J. M. Sancho, and A. H. Romero, *New J. Phys.* **7**, 29 (2005).
- [19] P. Reimann, C. Van den Broeck, H. Linke, P. Hänggi, J. M. Rubi, and A. Pérez-Madrid, *Phys. Rev. Lett.* **87**, 010602 (2001); *Phys. Rev. E* **65**, 031104 (2002).
- [20] B. Lindner, M. Kostur, and L. Schimansky-Geier, *Fluctuation Noise Lett.* **1**, R25 (2001).

- [21] E. Heinsalu, R. Tammelo, and T. Örd, *Phys. A (Amsterdam, Neth.)* **340**, 292 (2004).
- [22] I. G. Marchenko, I. I. Marchenko, and A. V. Zhiglo, *Eur. Phys. J. B* **87**, 10 (2014).
- [23] M. Evstigneev, O. Zvyagolskaya, S. Bleil, R. Eichhorn, C. Bechinger, and P. Reimann, *Phys. Rev. E* **77**, 041107 (2008).
- [24] X.-g. Ma, P.-Y. Lai, B. J. Ackerson, and P. Tong, *Soft Matter* **11**, 1182 (2015).
- [25] I. G. Marchenko and I. I. Marchenko, *Europhys. Lett.* **100**, 50005 (2012).
- [26] *Dynamics at Solid State Surfaces and Interfaces*, edited by U. Bovensiepen, H. Petek, and M. Wolf (Wiley-VCH, Weinheim, 2010), Vol. 1; *The Chemical Physics of Solid Surfaces: Surface Dynamics*, edited by D. Woodruff (Elsevier, Amsterdam, 2003).
- [27] A. Kulemin, *Ultrasound and Diffusion in Metals* (Metallurgy, Moscow, 1978), in Russian.
- [28] D. Speer, R. Eichhorn, and P. Reimann, *Europhys. Lett.* **97**, 60004 (2012).
- [29] J. M. Sancho and A. M. Lacasta, *Eur. Phys. J.: Spec. Top.* **187**, 49 (2010).
- [30] I. G. Marchenko and I. I. Marchenko, *JETP Lett.* **95**, 137 (2012).
- [31] I. G. Marchenko and I. I. Marchenko, *J. Phys. Conf. Ser.* **514**, 012045 (2014).
- [32] J. Spiechowicz and J. Łuczka, *Phys. Rev. E* **91**, 062104 (2015).
- [33] A. M. Lacasta, J. M. Sancho, A. H. Romero, I. M. Sokolov, and K. Lindenberg, *Phys. Rev. E* **70**, 051104 (2004).
- [34] D. Kuznetsov, *Stochastic Differential Equations: Theory and Practice of Numerical Solution* (St. Petersburg Polytechnic University Press, St. Petersburg, 2010), in Russian.
- [35] B. Lindner and E. M. Nicola, *Phys. Rev. Lett.* **101**, 190603 (2008).
- [36] S. Saikia and M. C. Mahato, *Phys. Rev. E* **80**, 062102 (2009).
- [37] O. M. Braun, A. I. Volokitin, and V. P. Zhdanov, *Sov. Phys. Usp.* **32**, 605 (1989); J. V. Barth, *Surf. Sci. Rep.* **40**, 75 (2000).
- [38] L. W. Bruch, R. D. Diehl, and J. A. Venables, *Rev. Mod. Phys.* **79**, 1381 (2007); J. Krim, *Adv. Phys.* **61**, 155 (2012).
- [39] X. Liu, Y. Han, J. W. Evans, A. K. Engstfeld, R. J. Behm, M. C. Tringides, M. Hupalo, H.-Q. Lin, L. Huang, K.-M. Ho, D. Appy, P. A. Thiel, and C.-Z. Wang, *Prog. Surf. Sci.* **90**, 397 (2015); E. Durgun, S. Ciraci, and T. Yildirim, *Phys. Rev. B* **77**, 085405 (2008); H. Pinto and A. Markevich, *Beilstein J. Nanotechnol.* **5**, 1842 (2014); L. Madeira and S. A. Vitiello, *Surf. Sci.* **655**, 39 (2017).
- [40] J. Sone, T. Yamagami, K. Nakatsuji, and H. Hirayama, *Jpn. J. Appl. Phys.* **55**, 035502 (2016); V. Kumaresan, L. Largeau, A. Madouri, F. Glas, H. Zhang, F. Oehler, A. Cavanna, A. Babichev, L. Travers, N. Gogneau, M. Tchernycheva, and J.-C. Harmand, *Nano Lett.* **16**, 4895 (2016); L. Liu, Z. Chen, L. Wang, E. Polyakova (Stolyarova), T. Taniguchi, K. Watanabe, J. Hone, G. W. Flynn, and L. E. Brus, *J. Phys. Chem. B* **117**, 4305 (2013); P. Xu, L. Dong, M. Neek-Amal, M. L. Ackerman, J. Yu, S. D. Barber, J. K. Schoelz, D. Qi, F. Xu, P. M. Thibado, and F. M. Peeters, *ACS Nano* **8**, 2697 (2014).
- [41] J. H. Weaver and G. D. Waddill, *Science* **251**, 1444 (1991); J. S. Palmer, P. Swaminathan, S. Babar, and J. H. Weaver, *Phys. Rev. B* **77**, 195422 (2008).
- [42] A. V. Krasheninnikov, K. Nordlund, P. O. Lehtinen, A. S. Foster, A. Ayuela, and R. M. Nieminen, *Phys. Rev. B* **69**, 073402 (2004); A. D. Migone, in *Adsorption by Carbons*, edited by E. Bottani and J. M. D. Tascon (Elsevier, Amsterdam, 2007), Chap. 16, p. 403; S. M. Gatica, M. M. Calbi, R. D. Diehl, and M. W. Cole, *J. Low Temp. Phys.* **152**, 89 (2008).
- [43] M. Jafary-Zadeh, C. D. Reddy, and Y.-W. Zhang, *Phys. Chem. Chem. Phys.* **16**, 2129 (2014).
- [44] J. Huot, in *New Trends in Intercalation Compounds for Energy Storage*, edited by C. Julien, J. P. Pereira-Ramos, and A. Momchilov (Springer, Dordrecht, 2002), pp. 109–144.
- [45] D. P. Broom, *Hydrogen Storage Materials: The Characterisation of Their Storage Properties* (Springer, London, 2011); R. A. Varin, T. Czujko, and Z. S. Wronski, *Nanomaterials For Solid State Hydrogen Storage*, Fuel Cells and Hydrogen Energy (Springer, New York, 2009).
- [46] G. Grynberg and C. Robilliard, *Phys. Rep.* **355**, 335 (2001); M. Zelan, H. Hagman, G. Labaigt, S. Jonsell, and C. M. Dion, *Phys. Rev. E* **83**, 020102 (2011).
- [47] C. I. Duruöz, R. M. Clarke, C. M. Marcus, and J. S. Harris, Jr., *Phys. Rev. Lett.* **74**, 3237 (1995); N. E. Staley, N. Ray, M. A. Kastner, M. P. Hanson, and A. C. Gossard, *Phys. Rev. B* **90**, 195443 (2014).